Structural insights from high-resolution diffusion tensor imaging and tractography of the isolated rat hippocampus

Timothy M. Shepherd,[a,*] Evren Özarslan,[b] Michael A. King,[a,c]
Thomas H. Mareci,[d] and Stephen J. Blackband[a,e]

[a]Department of Neuroscience, McKnight Brain Institute, University of Florida, Gainesville, FL 32610, USA
[b]Department of Computer and Information Science and Engineering, University of Florida, Gainesville, FL 32611, USA
[c]Medical Research Service, Malcolm Randall VA Medical Center, Gainesville, FL 32602, USA
[d]Department of Biochemistry and Molecular Biology, University of Florida, Gainesville, FL 32610, USA
[e]National High Magnetic Field Laboratory, Tallahassee, FL 32310, USA

The hippocampus is a critical structure for learning and memory formation injured by diverse neuropathologies such as epilepsy or Alzheimer's disease. Recently, clinical investigations have attempted to use diffusion tensor MRI as a more specific surrogate marker for hippocampal damage. To first better understand the tissue architecture of healthy hippocampal regions, this study characterized 10 rat hippocampi with diffusion tensor imaging (DTI) at 50-μm in-plane image resolution using a 14.1-T magnet. Chemical fixation of the dissected and straightened rat hippocampus provided a simple, effective way to reduce partial volume effects when segmenting hippocampal regions and improved mean signal-to-noise per unit time (e.g. 50.6 ± 4.4 at $b = 1250$ s/mm^2 in 27 min). Contrary to previous reports that water diffusion is homogeneous throughout the nervous system, statistically different mean diffusivities were observed (e.g. 0.238 ± 0.054 and 0.318 ± 0.084 μm^2/ms for the molecular and granule cell layers respectively) (ANOVA, $P < 0.05$). Different hippocampal subregions had lower fractional anisotropy than uniformly fibrous structures like corpus callosum because of their complex architecture. DTI-derived color fiber orientation maps and tractography demonstrated most components of the trisynaptic intrahippocampal pathway (e.g. orientations in stratum lacunosum–moleculare were dominated by perforant and Schaffer fibers) and also permitted some assessment of connectivity in the rat hippocampus.
© 2006 Elsevier Inc. All rights reserved.

Introduction

The hippocampus is an important structure for semantic and episodic memory formation that is particularly vulnerable to acute or chronic injury (Amaral and Witter, 1995; Squire et al., 2004). Memory impairment from hippocampal damage or connected limbic structures often results in devastating effects on a patient's day-to-day coping skills and quality-of-life (e.g. Alzheimer's disease) (Larson et al., 1992). Better imaging-based surrogate markers are needed to understand how different disease processes structurally alter the hippocampus and damage its function and to provide better clinical tools for the diagnosis and prognosis of hippocampal disease. Previous clinical MRI research studies have described volumetric changes associated with progressive hippocampal atrophy in Alzheimer's disease and other pathologies (Woermann et al., 1998), but these findings were nonspecific. Alternatively, in the past 10 years, diffusion tensor imaging (DTI) has been used to better characterize coherent fiber structures in nervous tissue (Basser and Jones, 2002). This alternative to conventional MRI contrast methods may better characterize disease-specific microstructural changes to the injured hippocampus (Van Hoesen and Hyman, 1990). Higher image resolutions also are likely to help distinguish hippocampal diseases since certain regions of the hippocampus are selectively vulnerable to particular diseases (e.g. hypoxia specifically damages the CA1 subregion) (Schmidt-Kastner and Freund, 1991; Spielmeyer, 1925).

In addition to its clinical importance, the hippocampus has provided an intriguing structure for fundamental cytoarchitectural investigations ever since the classic descriptions by Cajal, Golgi and Lorente de No (Fig. 1) (Cajal, 1911; Golgi et al., 2001; Lorente de No, 1934). In particular for this study, the hippocampus provides an interesting tissue substrate for MRI investigations because it is phylogenetically older than cortex and has atypical microstructure compared to the gray or white matter typically studied with DTI methods. The hippocampus contains distinct layers; densely packed neuron cell body layers like the stratum pyramidale are surrounded by layers of neuropil, such as stratum radiatum, where relatively few neuron cell bodies are interspersed with glia and a complex interdigitation of dendrites and axonal projections (Amaral and Witter, 1989; Duvernoy, 1998). The hippocampus also contains several well-described neuronal circuits

* Corresponding author. Fax: +1 352 392 3422.
E-mail address: tms@mbi.ufl.edu (T.M. Shepherd).
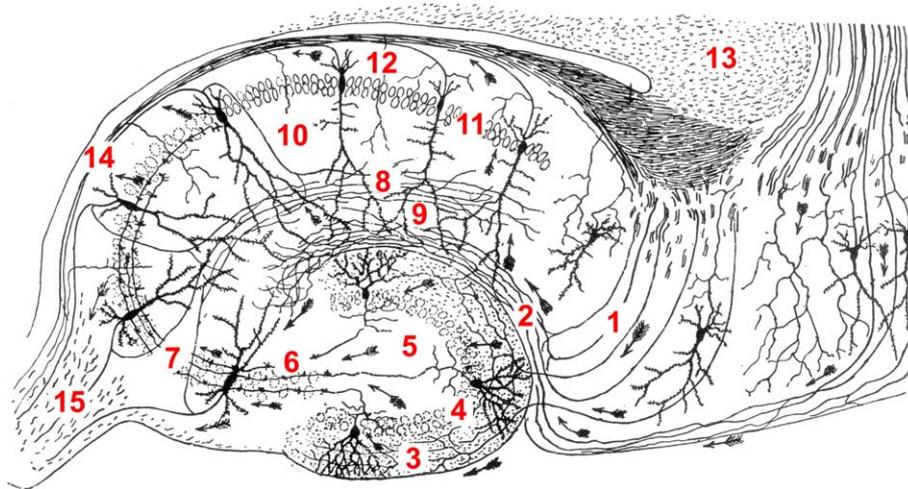**Available online on ScienceDirect (www.sciencedirect.com).**

Fig. 1. Hippocampal anatomy and connectivity depicted by Cajal (1911) based on the silver chromate method, which only stains a limited number of neurons. Here, Cajal used arrows to demonstrate the fiber connectivity of the trisynaptic pathway in the hippocampus. In this circuit, entorhinal cortex neurons innervate dentate granule neuron dendrites via the perforant pathway. Granule cell axons, called mossy fibers, then project to CA3 pyramidal neurons. A diffuse projection of CA3 axons forms the Schaffer collateral system innervating the CA1 strata radiatum and oriens. Finally, axons from CA1 and CA3 project via the alveus to the fimbria. The orientation and localization of these pathways define anatomical layers within the hippocampus [1 = subiculum, 2 = perforant pathway axons, 3 = molecular layer, 4 = granule cell layer, 5 = hilum, 6 = mossy fiber axons, 7 = CA3 pyramidal neurons, 8 = Schaffer collateral axons, 9 = stratum lacunosum–moleculare, 10 = stratum radiatum, 11 = CA1 pyramidal neurons, 12 = stratum oriens, 13 = dorsal hippocampal commissure, 14 = alveus, 15 = fimbria].

like the trisynaptic intrahippocampal pathway (Fig. 1), which is linked to semantic memory formation (Squire et al., 2004) and thus provides an interesting structure for fundamental investigations into memory-related disorders such as Alzheimer's disease. The trisynaptic pathway contains several coherent neuronal pathways such as Schaffer collaterals, perforant and mossy fibers (Witter et al., 2000) that are significantly smaller and more heterogeneous than the typical white matter fiber bundles studied previously with DTI and tractography methods (e.g. corpus callosum) (Wakana et al., 2004). These smaller structures provide an interesting challenge to MRI and may help us to understand the capabilities and limitations to characterizing neuronal fiber coherences using particular water diffusion measurement protocols even when very high spatial resolutions are attainable.

Not surprisingly, then, previous investigations have been eager to characterize aspects of the normal and injured hippocampus with diffusion tensor imaging at high spatial resolutions. Some of the best results have come when the rodent hippocampus was studied in situ with diffusion MRI using formaldehyde-fixed C57BL/6J mouse brains (Benveniste et al., 2000; Zhang et al., 2002). These studies benefited from very long scan times and high-field magnets to improve SNR for diffusion-weighted imaging with improved spatial resolutions. However, unlike the human hippocampus, the in situ rodent hippocampus is C-shaped and oriented oblique to the standard sagittal, axial and coronal divisions of the whole brain. Analysis in these standard reference planes is thus likely to result in more voxels that include multiple tissue architectures. Furthermore, some layers of the rodent hippocampus are less than 100 µm thick when examined histologically perpendicular to the septo-temporal axis (Paxinos and Watson, 1986; Pellegrino and Cushman, 1967). With insufficient resolution and significant partial volume effects from the hippocampus' curving in situ orientation, observation of the intrinsic DTI properties of particular hippocampal layers may be confounded. Furthermore, this problem also may reduce the magnitude of observed change in hippocampal regions that are

selectively vulnerable to particular insults, thus limiting the specificity of DTI as a surrogate marker of hippocampal injury.

Such partial volume averaging problems might be overcome by obtaining diffusion tensor MRI data of the whole rodent brain at 25-µm isotropic resolution, but obtaining adequate signal-to-noise ratios (SNR) for such data is prohibitively demanding even with very high-field magnets. Alternatively, this study applied a novel approach to preparing hippocampi for high-resolution diffusion tensor imaging by surgically dissecting the anatomical structure of interest from perfusion-fixed rat brain. Similar to methods first described by Gaarskjaer (1978), the isolated hippocampi were chemically fixed with 4% formaldehyde in a linear orientation that preserved their internal structural characteristics. This axial straightening of the curved hippocampus permitted the use of MRI radiofrequency coils 3- to 4-fold smaller than required for MRI of the whole rat brain. The minimization of partial volume effects and improvements in SNR from these simple steps facilitated very high-resolution images for diffusion tensor analysis and tractography characterizations of the rat hippocampus and its component layers. These data led to several novel insights into this complicated structure and improved our understanding of the relationship between MRI-observed water diffusion and tissue microstructure.

Methods

Dissection of the rat hippocampus

The University of Florida Institutional Animal Care and Use Committee approved the use of laboratory animals for this study. Five adult male Long–Evans rats (200–250 g) were deeply anesthetized with isofluorane and euthanized by exsanguination during perfusion fixation. The rats were perfused through an intra-aortic cannula with saline containing heparin (10 IU/mL) then 4%

formaldehyde (from paraformaldehyde) in phosphate-buffered saline (PBS) (pH 7.4). The solutions were at room temperature, and the osmolality of the saline and PBS was 295 mosM/kg as measured by a freezing point depression osmometer (Precision Systems Inc.; Natick, MA). The rat brain was immediately removed by craniotomy and immersion-fixed for 30 additional minutes in fresh 4% formaldehyde solution at room temperature.

Each brain then was bisected mid-sagittally, and both hippocampi removed by a medial approach using the lateral ventricle (Alger et al., 1984). As shown in Fig. 2, the anatomical relationships of the hippocampus to other brain structures simplify its physical isolation. The rostral portions of the dorsal hippocampus are enveloped by the rat brain ventricles containing cerebrospinal fluid. Although some aspects of the fimbria and fornix appose diencephalon structures located more ventrally, only the fornix penetrates into this tissue rostrally at some remove from the
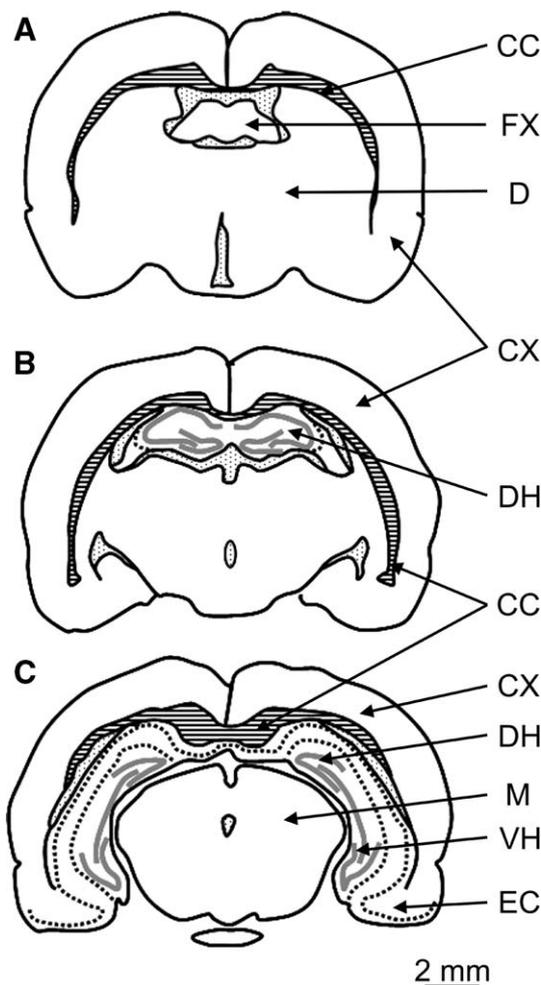

Fig. 2. Simplified line drawings (adapted from Pellegrino and Cushman, 1967) depicting coronal anatomy of the rat brain in situ at bregma (A), 1.8 mm caudal to bregma (B) and 3.8 mm caudal to bregma (C). The hippocampi have limited connections to brain parenchyma via the rostral extension of the fornices via the entorhinal cortex in the ventral–caudal brain and via midline intrahippocampal connections. Transection of these 3 connections isolates the hippocampus from the rest of the brain for high-resolution diffusion tensor MRI characterization [CC = corpus callosum, CX = cerebral cortex, D = diencephalon, DH = dorsal hippocampus, EC = entorhinal cortex, FX = fornix, M = mesencephalon, VH = ventral hippocampus].
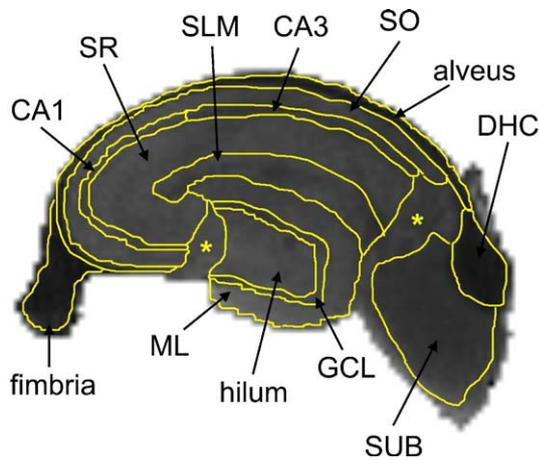
hippocampus (see Figs. 2A and B). Furthermore, the rat hippocampus is apposed, but not adherent to the corpus callosum and external capsule. This plane allows the dorsal surfaces of the ventral and dorsal hippocampus to be separated easily from brain parenchyma (see Figs. 2B and C). These advantageous anatomic features leave only 3 relatively small regions on the proximal and distal borders of the rat hippocampus where scalpel incisions were required for its isolation: the rostral fornix, the midline connection to the contralateral hippocampus and the ventral–caudal extension into the entorhinal cortex.

The isolated hippocampi varied between 10 and 12 mm in length depending on the points of transection for the septal and temporal poles. The septal and temporal halves of the hippocampus roughly correspond to the dorsal and ventral hippocampi. Once dissected, isolated hippocampi were placed in open-ended, thin-walled glass NMR tubes (~4 mm inner diameter and 2-cm long) such that the septo-temporal axis of the hippocampus was collinear with the long axis of the tube. A version of this process for "extending" the hippocampus to better analyze its 3D connectivity was first described by Gaarskjaer (1978). The samples then were immersion-fixed in fresh 4% formaldehyde solution for at least 8–10 days at 4°C prior to the MRI data collection.

Diffusion tensor MRI acquisition

For MRI experiments, the hippocampi were warmed gradually to room temperature and washed 4–5 times in PBS over a 24-h period to remove free formaldehyde, which can cause significant T_2 shortening in fixed tissue samples (Shepherd et al., 2005). The samples were then removed from the open-ended glass tubes with a polished glass rod and replaced into a normal length 5-mm NMR tube containing fresh PBS. It was essential to remove all air bubbles from the samples to prevent susceptibility artifacts; this was accomplished by carefully dislodging any bubbles on the sample surface with a 20-cm fine glass tip fashioned from an NMR pipette. The samples next were placed into a 5-mm Helmholtz-pair radiofrequency coil, and MRI data were acquired using a 14.1-T wide-bore spectrometer with 3000 mT/m diffusion gradients.

After pilot T_1- and diffusion-weighted images to locate sample position and orientation, a protocol for acquiring the diffusion tensor of the rat hippocampus was acquired. This protocol included acquisition of 22 images using a pulsed gradient spin echo pulse sequence with repetition time (TR) = 1.5 s, echo time (TE) = 28.3 ms, bandwidth = 35 kHz, field-of-view (FOV) = 4.5 × 4.5 mm, matrix = 90 × 90 with 20–30 continuous 200-μm-thick axial slices (oriented transverse to the septo-temporal axis of the isolated hippocampus). After the first image set was collected without diffusion weighting (b ~0 s/mm^2), 21 diffusion-weighted image sets with gradient strength (G) = 415 mT/m, gradient duration (δ) = 2.4 ms, gradient separation (Δ) = 17.8 ms and diffusion time (T_d) = 17 ms were collected. Each of these image sets used different diffusion gradients (with approximate b values of 1250 s/mm^2) whose orientations were determined from the 2nd order tessellations of an icosahedron projected onto the surface of a unit hemisphere. The image without diffusion weighting had 36 signal averages (time = 81 min), and each diffusion-weighted image had 12 averages (time = 27 min per diffusion gradient orientation) to give a total imaging time of 10.8 h per hippocampus. Temperature was maintained at 20 ± 0.2°C throughout the experiments using the temperature control unit of the magnet previously calibrated by methanol spectroscopy.

Fig. 3. Non-diffusion-weighted image of an isolated rat hippocampus demonstrated some T_2 contrast especially in hippocampal regions with significant white matter (fimbria, alveus and dorsal hippocampal commissure). Different architectural regions of the hippocampus were manually segmented (yellow boundaries) for quantitative analysis of FA and mean diffusivity [SR = stratum radiatum, SLM = stratum lacunosum–moleculare, SO = stratum oriens, DHC = dorsal hippocampal commissure, SUB = subiculum, GCL = granule cell layer, ML = molecular layer]. Regions that could not be segmented unambiguously were marked with "*" in the figure and excluded from the analysis.

MRI data analysis

The resulting data were fit to an apparent rank-2 diffusion tensor at each voxel from which non-diffusion-weighted, mean diffusivity ($<D>$), fractional anisotropy (FA) and fiber direction images were derived (Basser, 1995). Data from these calculations were used to create color fiber orientation maps. In addition, fiber tracts were calculated in ortho- and retrograde directions from selected seed points using a streamline-based algorithm that employs 4th-order Runge–Kutta technique (Basser et al., 2000; Press et al., 1992).

The different region-of-interests (ROI) in the rat hippocampus were manually segmented using the non-diffusion-weighted images with custom-built computer software. These regions were identified and prescribed based on anatomical literature (Amaral and Witter, 1989) and included the stratum oriens, stratum pyramidale (CA1 and CA3), stratum radiatum, stratum lacunosum–moleculare in the hippocampus proper; the hilus, molecular and granule cell layers of the dentate gyrus; as well as the fimbria and subiculum (for segmentation boundaries, see Fig. 3). Quantitative data from the FA and $<D>$ images then were calculated using these ROIs. DTI values from the right and left hippocampi were compared first to determine if there were statistically significant differences between the 2 sides—none were observed so data from the 10 hippocampi were grouped together. Fractional anisotropy and mean diffusivity values for different laminar regions of the hippocampi were compared with a one-way analysis of variance (Sigmastat 2.03, SPSS, Inc., San Rafael, CA). Statistically significant differences between particular regions were subsequently assessed using a Tukey multiple comparisons test. Significance for all statistical tests was predetermined at $P < 0.05$.

Signal-to-noise ratios (SNR) for individual diffusion-weighted images were calculated based as the mean signal in the rat hippocampus (minus the mean noise signal) divided by the standard deviation of the noise signal. The noise signal was obtained from an ROI drawn in the upper corner of the image field-of-view outside the sample and away from potential phase encode artifacts. In each dataset, an ROI drawn in the PBS solution also was used to obtain fractional anisotropy and mean diffusivity of isotropic water as an internal control for assessing data quality, temperature stability and gradient calibration.

Results

Isolation of 10 hippocampi from 5 rats was simple due to the limited anatomical connections of the rat hippocampus to apposed brain structures (Fig. 2), and the ease by which the formaldehyde-fixed structure is extended into a cylindrical shape shortly after perfusion fixation of the whole rat. This preparation did not damage the hippocampus (Fig. 4) and facilitated the collection of high quality diffusion-weighted MRI data for subsequent rank-2 diffusion tensor analysis (Fig. 5). The mean diffusivity for PBS surrounding the hippocampal samples (1.809 ± 0.102 μm^2/ms) was similar to published values of water at room temperature (Harris and Woolf, 1980), and the fractional anisotropy for PBS was 0.070 ± 0.010. It should be noted that even at very low noise levels there may appear to be some anisotropy because of the nonlinear relationship between FA and the variance of the diffusion tensor eigenvalues (Özarslan et al., 2005). These values indicate that magnet bore temperature was stable throughout the experiment and that the diffusion gradients were calibrated well. Mean SNR for the isolated rat hippocampi in the diffusion-weighted MRI images at 50-μm in-plane resolution were excellent with 103.4 ± 11.0 and 50.6 ± 4.4 at $b = 0$ s/mm^2 and 1250 s/mm^2 respectively. Fig. 5 also demonstrated that even simple diffusion-weighted images can reflect the regional heterogeneity of the rat hippocampus. Apparent diffusion coefficients appear low in the white matter regions of the hippocampus (fimbria, alveus and dorsal hippocampal commissure) and high in regions of densely packed neuronal soma (granule cell, CA1 and CA3 pyramidal neuron layers).

High quality diffusion tensor datasets were generated from these diffusion-weighted images (Fig. 6). These data then were
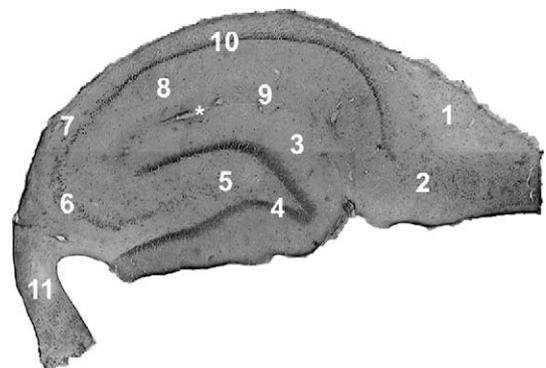

Fig. 4. Tiled histology image from the midsection of an isolated rat hippocampus used for this study (H&E, original magnification 4×). Most of the laminar anatomy of the rat hippocampus can be recognized with this standard, simple histology stain [1 = dorsal hippocampal commissure, 2 = subiculum, 3 = molecular layer, 4 = granule cell layer, 5 = hilum, 6 = CA3 pyramidal neurons, 7 = stratum oriens, 8 = stratum radiatum, 9 = stratum lacunosum–moleculare, 10 = CA1 pyramidal neurons, 11 = fimbria]. Remnants of the residual hippocampal sulcus (*) can be seen between the stratum lacunosum–moleculare and the molecular layer. None of the hippocampi appeared to be damaged by the isolation procedure.
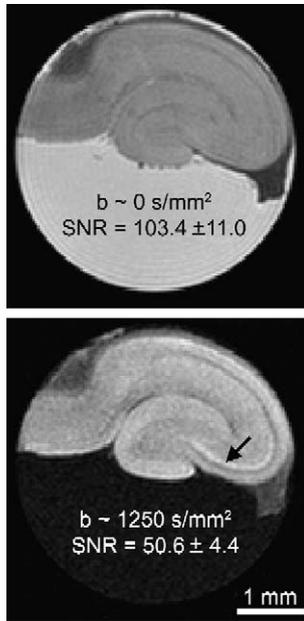
Fig. 5. Examples of 50-μm in-plane resolution, diffusion-weighted images used to calculate the rank-2 diffusion tensor for different regions of the isolated rat hippocampus. The signal-to-noise ratios (SNR) in these images were excellent for subsequent diffusion tensor analysis [mean ± SD, 10 hippocampi]. In this particular diffusion-weighted image (bottom panel), some mossy fiber convergence at the apical dendrites of CA3 (i.e. the stratum lucidum) was evident as a slender region of increased diffusion restriction at the distal end of the CA3 pyramidal neuron layer (black arrow). Diffusion-weighted hyperintensities also can be noted for the alveus and perforant fibers in the outer 2/3 of the infrapyramidal molecular layer where coherent fibers also run perpendicular to this particular diffusion gradient orientation.

used to generate parameter maps of no diffusion weighting, mean diffusivity ($<D>$) and fractional anisotropy (FA) (Fig. 7). With these MRI contrasts, there was no evidence of gross morphological damage or distortion at any transverse level in the septo-temporal axis of the extended hippocampus in the 10 samples (Fig. 8). Different architectural regions of the hippocampus changed size and shape from the septal to temporal poles of the hippocampus. The hippocampus becomes thicker, especially in the dentate gyrus, as the temporal pole is approached due to more input from the entorhinal cortex via the perforant pathway. Conversely, the white matter structures of the fimbria and the dorsal hippocampal commissure accumulate towards the septal pole to become the fornix and connection to the contralateral hippocampus respectively. Movies of fractional anisotropy (Video 1), mean diffusivity (Video 2) and color fiber orientation maps (Video 3) that scroll through the entire septo-temporal axis of a selected rat hippocampi from this study can be found online.

Non-diffusion-weighted images demonstrated enough detail for manual ROI segmentation of the different regions and suggested that there were some significant T_2 differences between different regions of the rat hippocampus (Fig. 3). Mean diffusivity images demonstrated similar contrast relationships as first suggested by simple diffusion-weighted images (Fig. 5), but also accounted for the potentially confounding effects of diffusion anisotropy and T_2 differences. Three distinct tissue diffusivities can be observed from these images (Fig. 7) with mean water diffusivities slowest in the white matter structures, faster in the neuropil layers and fastest in

the densely packed neuronal layers. The quantization of these differences is discussed further below.

Fractional anisotropy maps demonstrated several fine anatomical details and laminar divisions of the rat hippocampus that were not readily observed with the non-diffusion-weighted or mean diffusivity images (Fig. 7). Furthermore, Fig. 8 demonstrated the changes in laminar thickness and FA throughout the septo-temporal axis of the rat hippocampus. The diffusion anisotropy and thickness of the stratum radiatum increased towards the temporal end of the hippocampus. In contrast, the highly anisotropic, but smaller dorsal hippocampal commissure and fimbria structures accumulate towards the septal hippocampus to communicate with other structures in the rat brain. Fiber orientation color maps (Fig. 9), based on the principal eigenvector from the DTI data, also provided excellent anatomical contrast for the different hippocampal layers. The combination of DTI-derived FA and color fiber orientation maps were more effective together than either alone for discrimination of the underlying anisotropic structures for particular layers of the hippocampus (see Discussion). Simple DTI-derived tractography (Fig. 10) also could be used to aid assessment of the dominant anisotropic structures in particular hippocampal lamina. In some instances, tractography was able to ascribe multi-neuron connectivity in the rat hippocampus—for example, detailing some aspects of the trisynaptic pathway in Fig. 10 when the apical dendrites of the CA3 pyramidal neuron layer were used to seed the tract tracing. However, the full trisynaptic pathway was difficult to delineate because certain regions of the hippocampus that this memory circuit traverses, such as hilus, appear relatively isotropic to the relatively simple rank-2 tensor data analysis methods and tractography algorithms used (Fig. 7).

Mean diffusivity and FA for many different laminar regions of the rat hippocampus were statistically different (ANOVA, $P < 0.05$) (Table 1). Combined mean diffusivity for white matter structures in the rat hippocampus (fimbria and dorsal hippocampal commissure) (0.136 μm^2/ms) was 63% lower than the combined mean diffusivity of regions with densely packed neuronal bodies (granule cell, CA1 and CA3 neuron layers) (0.318 μm^2/ms). Another thin, superficial white matter structure, the alveus, had comparatively high diffusivity (0.277 ± 0.117 μm^2/ms) that probably reflects partial volume effects with adjacent PBS. Alternatively, neuropil-rich regions (molecular layer, hilus, stratum oriens, stratum radiatum, stratum lacunosum–moleculare and subiculum), which lack large white matter bundles or substantial numbers of neuronal soma, had combined mean diffusivities in between these two types of tissue architecture (0.238 μm^2/ms). The FA values also reflected differences between these different generalized microstructure types. No statistically significant differences were observed for DTI-derived parameters between the right and left hippocampi ($N = 5$ each, ANOVA, $P > 0.05$).

Discussion

Dissected isolation of the rat hippocampus for MRI characterization

The isolation and extension of the rat hippocampus optimize the structure's shape for small radiofrequency coils (e.g. 5-mm coil for rat hippocampus) so that optimal SNR per unit time is generated. This represents the most efficient anatomical means of imaging the hippocampus, although alternative coil types might further
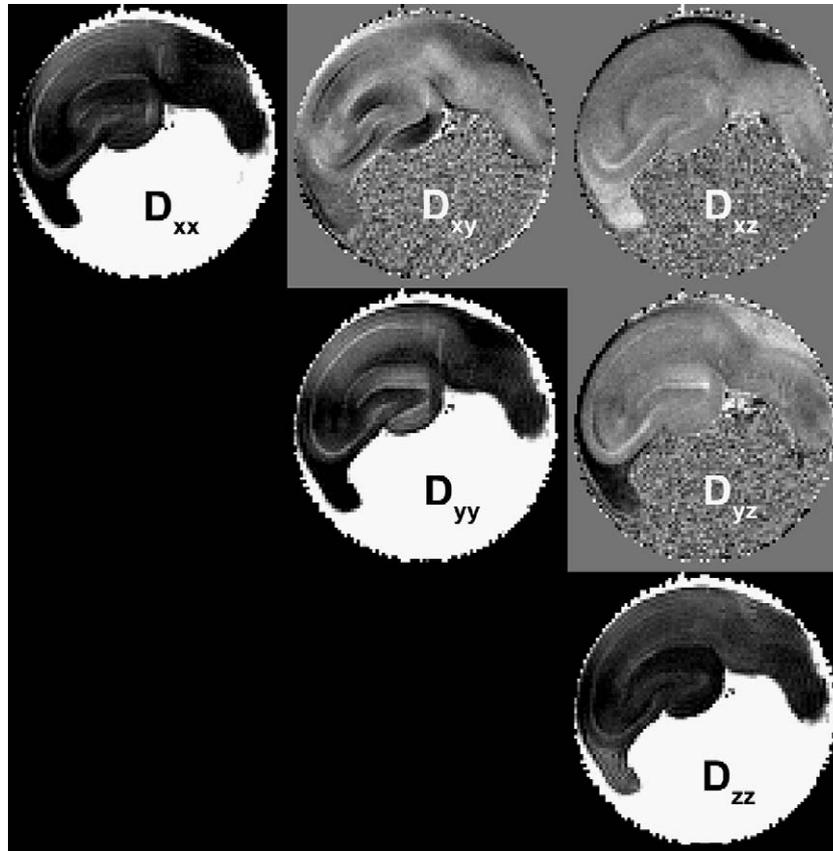
Fig. 6. Sample diffusion tensor dataset for a single MR-defined slice through the midpoint of the septo-temporal axis of an isolated rat hippocampus. The diagonal elements are scaled between the values of 0 and 0.0008 mm^2/s, whereas the off-diagonal elements are scaled between values of −0.0002 and 0.0002 mm^2/s.

improve SNR per unit time. This high SNR allowed the collection of 2-dimensional diffusion tensor MRI data with high in-plane resolution and reduced slice thickness ($50 \times 50 \times 200$ μm voxels). The extension of the rat hippocampus also reduces partial volume effects that may have confounded previous MRI characterizations of hippocampal substructures studied in situ (Benveniste et al., 2000; Zhang et al., 2002). Furthermore, the isolated rat hippocampus has an orientation that better correlates with the in situ anatomy of the human hippocampus, which, unlike rodent hippocampus, completes migration with the lateral telencephalic vesicle during its ontogeny so that the whole hippocampal structure is collinear with the axis of the lateral ventricle (Duvernoy, 1998).

The dissection and "extension" of the hippocampus do not damage its structure or connectivity as demonstrated by the initial studies of Gaarskjaer (1978). In fact, this approach has been used for tracer and lesion studies that have significantly improved understanding of the 3D intrinsic connectivity in the rodent hippocampus (Amaral and Witter, 1989). The lack of histologic (Fig. 4) or MRI signal changes suggestive of damage in the middle regions of the extended hippocampus (Fig. 8) further demonstrates that this method does not alter the internal hippocampal structure. Dissected isolation of the hippocampus, however, does prevent characterization of the brain structures that connect to the hippocampus via the rostral fornix, hippocampal commissure and
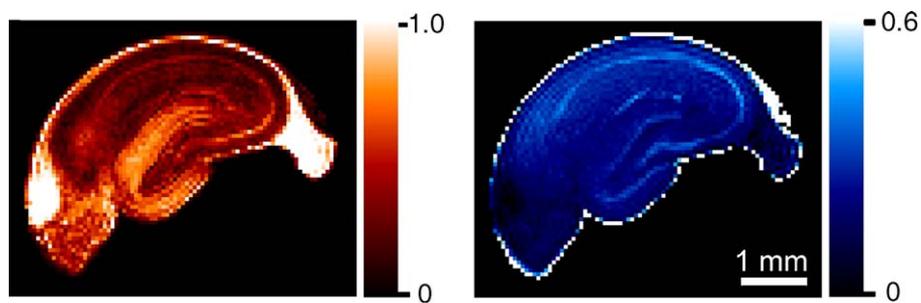

Fig. 7. Diffusion-tensor derived parameter maps of fractional anisotropy (red) and mean diffusivity (blue) for a selected rat hippocampus. The color scales are 0 to 1 for fractional anisotropy (no units) and 0 to 0.6 μm^2/ms for mean diffusivity. The map of fractional anisotropy provides excellent contrast resolution for many different regions of the hippocampus (see Discussion). At least 3 distinct mean diffusivities can be observed in diffusivity maps of the rat hippocampus (also see Table 1).
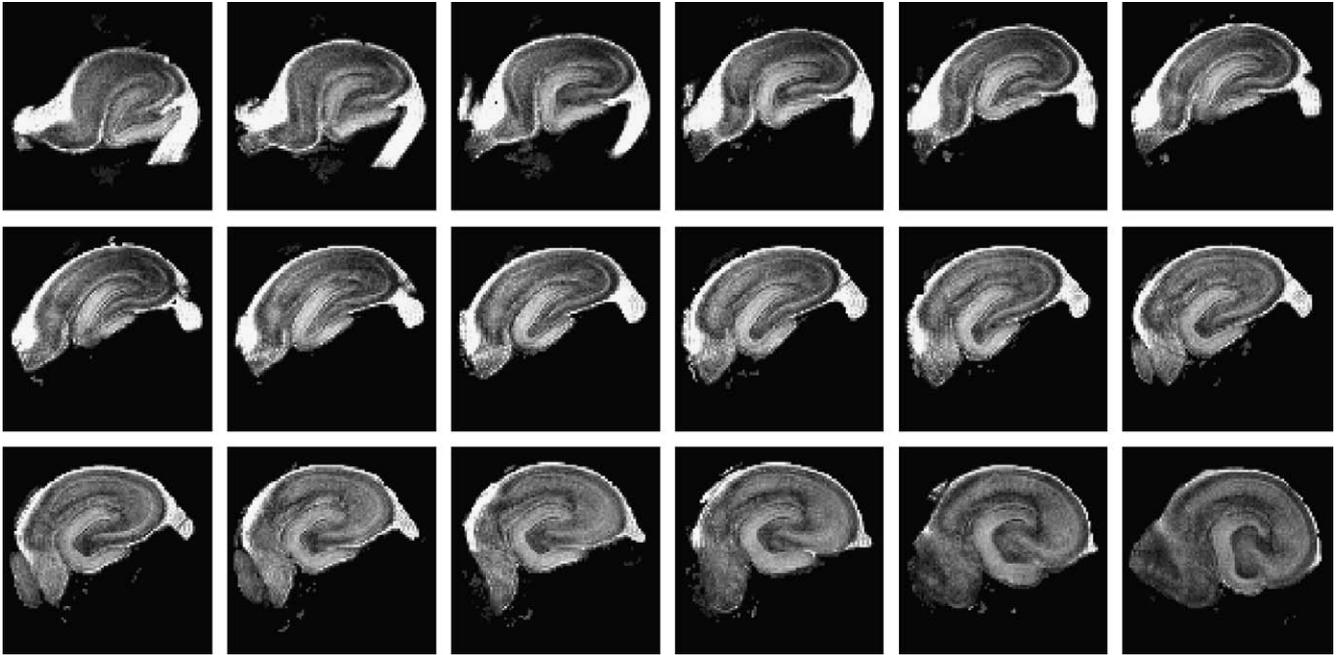
Fig. 8. 50-μm in-plane resolution fractional anisotropy images of an extended, isolated rat hippocampus. The series moves left-to-right from the septal end (upper left) to the temporal end (bottom right) of the hippocampus. For clarity, every other 200-μm-thick transverse MRI slice is shown and some additional images on either end were discarded. Different laminar regions of the hippocampus change their shape, size and magnitude of anisotropy from the septal to temporal poles of the hippocampus.

entorhinal cortex (Fig. 2). These large identifiable structures will be better characterized by whole brain diffusion MRI studies. Alternatively, one could sacrifice some SNR by using slightly larger radiofrequency NMR coils to include isolations of the hippocampus with selected connecting structures (e.g. the entorhinal cortex for characterizing the PS1/APP transgenic mouse model of Alzheimer's neuropathology).

Water diffusivity differences within the rat hippocampus

Contrary to previous MRI studies that suggested water diffusivity was homogeneous throughout the nervous system when anisotropy was accounted for (Basser and Jones, 2002; Pierpaoli and Basser, 1996), this study demonstrated statistically significant quantitative differences in mean water diffusivity between several regions of the rat hippocampus (see Fig. 7 and Table 1). This observation was qualitatively reported by Zhang et al. (2002). The relative differences in diffusion for the different lamina are likely to be valid for in vivo hippocampus despite fixation altering the absolute values obtained here (Shepherd et al., 2005). Such a conclusion is supported by comparable results obtained in unfixed, viable rat hippocampal slices with diffusion MRI (Shepherd et al., 2004) or with non-MRI methods, such as tetra-methyl ammonium (TMA) iontophoresis (McBain et al., 1990; Sykova et al., 2002). The mean diffusivity of water in nervous tissue appears to decrease significantly as the tissue architecture becomes volume-dominated by microscopic tubular structures such as axons and dendrites. The diffusion of water is most restricted in regions with relatively homogeneous collections of closely packed, myelinated axon bundles such as the fimbria. Conversely, regions of large, densely packed pyramidal or spherical-shaped neuronal soma (i.e. stratum pyramidale in CA1 and CA3, or stratum granulosum) have high mean water diffusivities. Intermediate values occur in neuropil,

where there are complex microscopic interdigitations of axons, dendrites and dendritic spines, such as the stratum radiatum. Diffusivity may correlate with the density of cellular membranes, cytoskeletal structures and/or myelin within a voxel. Thus, besides imparting anisotropy (Beaulieu, 2002), the restrictive effects of membranes also may impact the apparent diffusion coefficients of water. Even at these high spatial resolutions, some very thin layers within the hippocampus, such as the stratum granulosum, may still experience partial volume effects with adjacent layers that lead to underestimations of the true differences in mean water diffusivity between some hippocampal regions.

Differences in water diffusivity may best be explained by the improved spatial resolution of hippocampal layers in this study. The hippocampus is allocortex, which is distinguished from cerebral cortex (or isocortex) by its phylogenetically older tissue organization pattern. Thus, unlike isocortex, the hippocampus contains microarchitectural regions whose volumes are dominated by large neuronal soma (e.g. stratum pyramidale), neuropil (e.g. stratum lacunosum–moleculare) or a mixture of neuronal soma and neuropil (e.g. hilum). In contrast, histology of the different layers of the rat or human isocortex demonstrates a more heterogeneous admixture of these different microstructures (Paxinos and Watson, 1986). Layer-specific differences in the hippocampus can be recognized with histology or MR microscopy at high spatial resolutions (such as the present study), yet lower resolution MRI studies or in vivo studies are likely not to observe these distinctions.

Diffusion anisotropy and fiber orientation in the rat hippocampus

Understanding the DTI properties of the different regions of the normal rat hippocampus and their fiber connectivity is important since the hippocampus demonstrates selective regional vulnerabil-
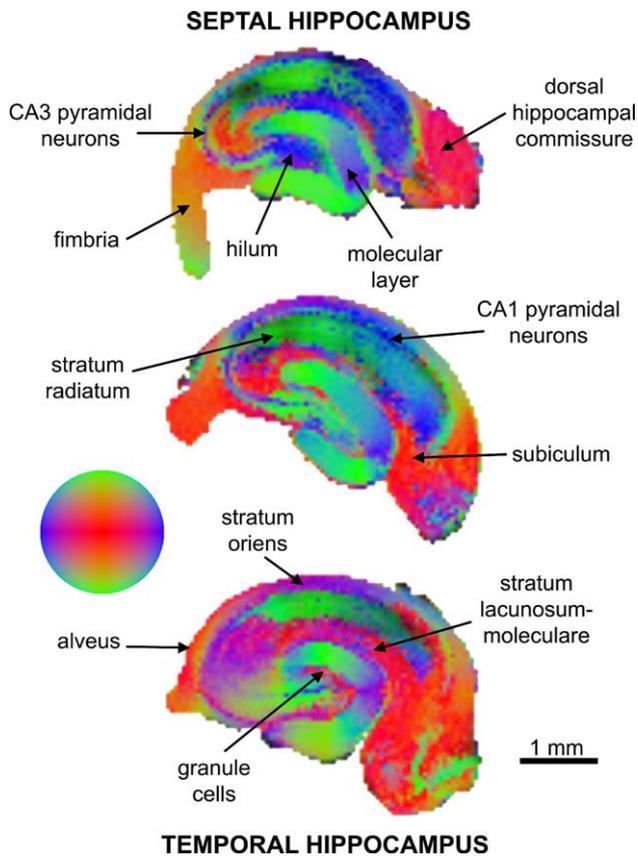
SEPTAL HIPPOCAMPUS

Fig. 9. DTI-derived color fiber orientation maps at the septal end (top), the midpoint (middle) and the temporal end (bottom) of an isolated rat hippocampus. The colorball indicates the direction of the principal eigenvector, which can be transverse (blue), vertical (green) or through the plane of the image parallel to the septo-temporal axis of the rat hippocampus (red). Fiber orientation for particular regions of the rat hippocampus can best be interpreted based on the orientations of axons and dendrites from neurons that compose the trisynaptic intrahippocampal pathway. For example, the radial diffusivities observed in the molecular layer of the dentate gyrus and the stratum radiatum of CA1 may be attributed to the large apical dendrites of granule cell and pyramidal neurons respectively (see Discussion for further details).

ity to particular disease processes (e.g. CA1 neuron death after hypoxia) (Schmidt-Kastner and Freund, 1991; Spielmeyer, 1925); this property could be used to increase the specificity of diffusion MRI. The primary structures that affect DTI contrast in the different lamina of the normal rat hippocampus are best assigned by considering information from both FA magnitude (Figs. 7 and 8) and the color fiber orientation maps (Fig. 9) in the context of neuron structure (Fig. 11) and in the context of previous literature describing the particular architectural features of each hippocampal lamina (e.g. Fig. 1) (Cajal, 1911; Duvernoy, 1998; Lorente de No, 1934; Witter et al., 2000). The orientation of fibers indicated in the color fiber orientation map (Fig. 9) can be interpreted based on the trisynaptic intrahippocampal pathway (Fig. 1) (Amaral and Witter, 1995; Duvernoy, 1998; Witter et al., 2000). For example, the highly anisotropic dorsal hippocampal commissure contains commissural fibers that run between the right and left hippocampi in a septo-temporal direction, which is congruent with their depiction in Fig. 9. Similarly, the high anisotropy in the fimbria can be assigned to efferent axons from CA1 and the subiculum,

along with afferent axons from the septal regions of the rat brain—these fibers also run parallel to the septal–temporal axis of the hippocampus. The thin alveus contains the efferent hippocampal fibers as they exit from the CA1 and subicular regions to wrap around the hippocampus in an oblique septal direction towards the fimbria and subsequently fornix. Although the stratum oriens first contains axons exiting the CA1 and CA3 neuronal layers into the alveus and fimbria, it has relatively low FA because it also contains the orthogonally oriented pyramidal neuron basal dendrite arborizations (Fig. 11).

In the pyramidal neuron layers underlying the stratum oriens, CA3 appears thicker and tends to have higher FA than the CA1 pyramidal neuron layer. However, in the temporal hippocampus (Fig. 8), FA cannot distinguish the CA1 or CA3 neuron layers from the adjacent stratum radiatum, although these layers are likely to lie between the contrasting color orientations for stratum oriens and radiatum in Fig. 9. In the septal hippocampus, it is still difficult to resolve the CA1 neuron layer, although the CA3 neuron layer appears to be delineated. This, however, may be due to mossy fiber input to CA3 (see Fig. 9) and the difficulty separating the true CA3 neuron layer from the stratum lucidum with simple rank-2 diffusion tensor analysis. The high anisotropy in the CA1 and CA3 pyramidal neuron layers reflects apical dendrites from the most basal pyramidal neurons (Fig. 11) (located adjacent to stratum oriens) projecting through the less basal neurons in route to stratum radiatum and beyond.

The apical dendrites of the CA1 and CA3 pyramidal neurons traverse the stratum radiatum and stratum lacunosum–moleculare (see Fig. 11). The stratum radiatum appeared relatively anisotropic and maintains radial fiber orientations from these pyramidal neuron apical dendrites (Fig. 9). Except for in the septal hippocampus, the stratum lacunosum–moleculare is less anisotropic than stratum radiatum as the apical dendrite diverges into its terminal arboriza-
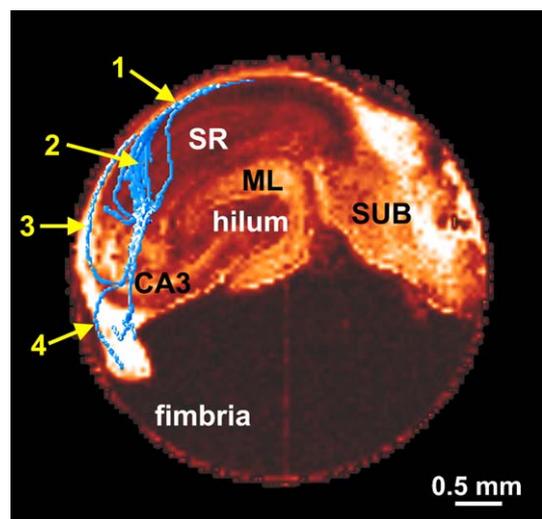

Fig. 10. Diffusion tensor tractography projected onto a fractional anisotropy image of the rat hippocampus may indicate intrahippocampal trisynaptic fiber projections (blue surfaces). This example could be interpreted to illustrate (1) axonal projections from the CA1 pyramidal neurons to the alveus, (2) divergent connections between the CA3 pyramidal neurons and the apical dendrites of CA1 neurons in the stratum radiatum, (3) axonal projections from the CA3 neurons to the alveus and (4) axonal projections from the CA3 neurons to the fimbria [SR = stratum radiatum, ML = molecular layer].

Table 1
Mean diffusivity and fractional anisotropy for different regions of the rat hippocampus [mean ± SD, 10 hippocampi]

Hippocampal region	Mean diffusivity (μm^2/ms)	Fractional anisotropy (no units)	Dominant anisotropic structure
Molecular layer	0.238 ± 0.054	0.526 ± 0.097	Granule cell apical dendrites
Granule cells	0.318 ± 0.084	0.530 ± 0.105	Granule cell apical dendrites
Hilum	0.245 ± 0.057	0.277 ± 0.075	Mossy fibers
CA3 stratum pyramidale	0.329 ± 0.056	0.386 ± 0.075	CA3 neurons and apical dendrites
CA1 stratum pyramidale	0.308 ± 0.056	0.373 ± 0.072	CA1 neurons and apical dendrites
Fimbria	0.164 ± 0.058	0.931 ± 0.054	CA1, CA3 and subicular axon projections
Alveus	0.277 ± 0.117	0.744 ± 0.075	Axon projections
Stratum oriens	0.238 ± 0.026	0.324 ± 0.056	Pyramidal neuron axons
Stratum radiatum	0.227 ± 0.041	0.322 ± 0.056	CA1 and CA3 neuron apical dendrites
Stratum lacunosum–moleculare	0.232 ± 0.042	0.315 ± 0.063	Perforant fibers
Subiculum	0.250 ± 0.056	0.310 ± 0.046	
Dorsal hippocampal commissure	0.109 ± 0.004	0.909 ± 0.097	Interhippocampal fibers
Whole hippocampus	0.241 ± 0.047	0.428 ± 0.093	NA
1-way ANOVA (P value)	<0.001	<0.001	NA

tions (Fig. 11). In the stratum lacunosum–moleculare, the apical dendrite may be masked by perforant fibers projecting orthogonally to its terminal arborizations. Normally, the division between the stratum moleculare and lacunosum is not recognized in rodent hippocampus (Duvernoy, 1998), but in the temporal end of the hippocampus, there is a thinner band of higher FA adjacent to the isotropic line of the vestigial hippocampal sulcus that may represent more distinct fiber coherences from the perforant pathway (Fig. 8), which is found predominantly in the stratum moleculare. In the color fiber orientation map of the septal hippocampus, this region of high FA is oriented parallel to the hippocampal sulcus as would be expected for the perforant pathway (Fig. 9).

Contrasts in the fiber color orientation map are particularly striking for separating the subiculum from the adjacent CA1 subregion—in the temporal end of the hippocampus, the anisotropic subiculum is separated from the CA1 by a band of isotropic
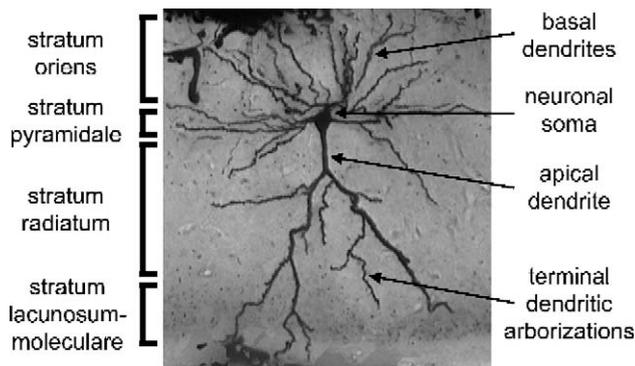

Fig. 11. Golgi-stained section demonstrating pyramidal neuron architecture within the CA1 region of rat hippocampus. Diffusion anisotropy and fiber orientations observed for rat hippocampus can be interpreted based on this pyramidal neuron architecture stratified into distinct layers (see Discussion). Anisotropy in the CA1 pyramidal layer (Fig. 7) and radial fiber orientations observed in the stratum radiatum (Fig. 9) are likely due to the parallel alignment of large-diameter primary apical dendrites from CA1 pyramidal cells. Distally in the stratum lacunosum–moleculare, the distal branches of these dendrites arborize in more random orientations such that FA decreases and the fiber orientation is instead dominated by orthogonally oriented perforant fibers from the entorhinal cortex. Similar interpretations can be made for other regions of the rat hippocampus, such as CA3, the dentate gyrus and subiculum.

diffusion (Fig. 8). Differences in FA also can be used to separate the subicular complex into prosubiculum (low FA), subiculum (high FA) and parasubiculum (low FA) in the more septal parts of the hippocampus. FA in the outermost layer of the subicular cortex is quite pronounced except in the temporal end of the hippocampus. The magnitude of anisotropy of the underlying layers of the subiculum also changes along the septo-temporal axis of the hippocampus but, when present, appears to be dominated by orientations parallel to the septo-temporal axis.

Similar to the subiculum, the hilar region of the dentate gyrus was easily distinguished from the CA3 subregion of the hippocampus proper, but this structure did not have high FA except for central extension of CA3 into the hilus, which likely represents the stratum lucidum, a region containing the mossy axonal fibers projecting from granule cells (see the septal hippocampus in Fig. 9). Anisotropy in the granule cell layer itself can be explained similarly to the CA1 and CA3 neuron layers— basal dendrites from the deepest granule cells in this lamina will extend through the densely packed, more superficial granule cells in route to the molecular layer, thus increasing the granule cell layer's FA. Conversely, mossy fibers from the most superficial granule cells will traverse the layer in the opposite direction towards the hilus and CA3 neurons but have a similar effect on granule cell layer FA and fiber orientation. The molecular layer also was highly anisotropic (Figs. 7 and 8), and its principal orientations appear dominated by the radial extensions of these granule cell dendrites into the molecular layer (Fig. 9). The observed radial pattern of fiber orientation, however, does not transition smoothly at the crest of the molecular layer, suggesting that the rank-2 diffusion tensor analysis may be detecting the coherent penetration of the perforant pathway into the dentate gyrus (e.g. the blue band in the molecular layer of Fig. 9). FA is lower at this point too, which may represent artificial reductions in FA from the crossing of granule cell dendrites and perforant fibers. FA intensity maps appear to further divide the molecular layer into inner and outer layers that may correspond to inputs from the commissural/septal fibers or the perforant pathway respectively (Fig. 7). Alternatively, this division may relate to decreased anisotropy from the terminal arborizations of granule cell dendrites as they terminate in the outer molecular layer.

As described above, in hippocampal regions where the anatomical literature indicates multiple fiber coherences may be encountered within the same voxel, the simple rank-2 diffusion

tensor analysis often emphasized the most dominant fiber coherence in the color fiber orientation map. Similarly, this type of analysis may underestimate the FA in certain hippocampal lamina by its inability to distinguish voxels containing relatively isotropic regions from regions with two or more crossing fiber coherences. Future MRI studies of diffusion anisotropy and orientation in the rat hippocampus may benefit from more advanced methods discussed further below.

Diffusion tractography of the rat hippocampus

Despite some limitations to the relatively simple rank-2 tensor analysis, the characterization of the isolated rat hippocampus enabled tractography at resolutions approximately an order of magnitude higher than previously described. In Fig. 10, several important components of the trisynaptic pathway including the Schaffer collaterals, CA1 and CA3 efferent axons were elicited. This example also demonstrated some divergences in the connections between different components of the trisynaptic pathway—both in the image plane and along the septo-temporal axis (not shown) (Amaral and Witter, 1989). This trisynaptic hippocampal circuit is critical for semantic memory formation (Amaral and Witter, 1995; Duvernoy, 1998; Squire et al., 2004). Future assessments of this circuit's integrity with DTI-derived maps and tractography may facilitate a better understanding of how the neuropathological hallmarks of Alzheimer's disease (beta-amyloid plaques and neurofibrillary tangles) disrupt the hippocampus' ability to form new memories. However, the full trisynaptic pathway was difficult to delineate because certain regions of the hippocampus that this memory circuit traverses, such as the hilus, appeared relatively isotropic to the rank-2 tensor analysis methods and the tractography algorithms used (Fig. 7). Clearly, future refinements will be required to realize this application's full potential for novel structural insight into the normal and injured rat hippocampus.

It also is important to note that the interpretations of DTI-derived tractography results, as well as FA and color fiber orientation maps, for the rat hippocampus were based on the architectural features of neurons (Fig. 11) and their spatial relationships within the different hippocampal layers as described by previous literature. Future MRI studies of the rodent hippocampus would greatly benefit from more direct histological correlations in the same hippocampal samples, although reliable, consensus methods for correlating connectivity have not yet been developed. This problem remains a challenging, but active area of research beyond the scope of this present work. As such, some assignments in this MRI characterization of rat hippocampus must be considered hypotheses. It should also be noted that diffusion imaging of the hippocampus could move beyond simply confirming neuroanatomical pathways recognized previously with other experimental techniques and demonstrate connectivities not previously known. Such information, however, may prove particularly difficult to verify.

Future directions

Diffusion MRI of the isolated, extended rodent hippocampus can be used to study a variety of different hippocampal pathologies in animal models. The improved spatial resolution and reduction in partial volume effects inherent to this preparation demonstrate potential for future MRI studies to characterize particular regions of the hippocampus that are selectively vulnerable to particular disease processes, such as the subiculum in Alzheimer's disease (Van Hoesen and Hyman, 1990), the CA1 region in hypoxia (Schmidt-Kastner and Freund, 1991; Spielmeyer, 1925) or the mossy fibers and granule cell layer in epilepsy (Nadler, 2003; Sutula et al., 1989; Tauck and Nadler, 1985). In addition to diffusion MRI studies, the methods described in this study can be used on rodent hippocampi for characterizations based on alternative MRI contrast mechanisms such as T_1- or T_2-weighted imaging or volumetric studies based on high-resolution gradient echo images. Such characterizations could supplement current efforts to develop whole brain atlases (Ma et al., 2005) or improve the quality of genetic knockout studies of brain development in mice (Benveniste et al., 2000) by generating highly detailed information for the hippocampus and its substructures.

High MRI spatial resolutions may be used to resolve increasingly small architectural regions of the nervous system (e.g. stratum granulosum in this study), but results from this study also suggest that increasing spatial resolution to improve characterization of the more complicated fiber structures in the brain with rank-2 diffusion tensor analysis is not alone sufficient. At higher resolutions, diffusion MRI studies then detect and/or are influenced by even smaller coherent pathways or smaller parcellations of "large" pathways. For example, clinical diffusion tensor MRI can detect the fornix of the in vivo human hippocampus but fails to demonstrate the granule cell dendrite coherences in the molecular layer noted by this study at higher resolutions. The same paradigm probably holds for subsequent studies at even higher spatial resolutions than presented here. Alternative methods of measuring diffusion anisotropy, such as high angular resolution diffusion imaging (Tuch et al., 2002), may be required to further improve our understanding of those rat hippocampal regions where multiple coherent fiber pathways exist at the length scales of particular image resolutions. These methods may provide better estimates of diffusion anisotropy and depict crossing fibers in regions such as the stratum lucidum where mossy fibers and the apical dendrites of CA3 neurons interdigitate orthogonally.

Appendix A. Supplementary data

Supplementary data associated with this article can be found, in the online version, at doi:10.1016/j.neuroimage.2006.04.210.

References

Alger, B.E., Dhanjal, S.S., Dingledine, R., Garthwaite, J., Henderson, G., King, G.L., Lipton, P., North, A., Schwartzkroin, P.A., Sears, T.A., Segal, M., Whittingham, T.S., Williams, J., 1984. Brain slice methods. In: Dingledine, R. (Ed.), Brain Slices. Plenum Press, New York, pp. 381–437.

Amaral, D.G., Witter, M.P., 1989. The three-dimensional organization of the hippocampal formation: a review of anatomical data. Neuroscience 31, 571–591.

Amaral, D.G., Witter, M.P., 1995. Hippocampal formation. In: Paxinos, G. (Ed.), The Rat Nervous System. Academic Press, New York, pp. 443–493.

Basser, P.J., 1995. Inferring microstructural features and the physiological state of tissues from diffusion-weighted images. NMR Biomed. 8, 333–344.

Basser, P.J., Jones, D.K., 2002. Diffusion-tensor MRI: theory, experimental design and data analysis—a technical review. NMR Biomed. 15, 456–467.

Basser, P.J., Pajevic, S., Pierpaoli, C., Duda, J., Aldroubi, A., 2000. In vivo fiber tractography using DT-MRI data. Magn. Reson. Med. 44, 625–632.

Beaulieu, C., 2002. The basis of anisotropic water diffusion in the nervous system—a technical review. NMR Biomed. 15, 435–455.

Benveniste, H., Kim, K., Zhang, L., Johnson, G.A., 2000. Magnetic resonance microscopy of the c57bl mouse brain. NeuroImage 11, 601–611.

Cajal, S.R., 1911. Histologie Du Systeme Nerveux De L'Homme Et Des Vertebretes. A. Maloine, Paris.

Duvernoy, H.M., 1998. The Human Hippocampus, 2nd ed. Springer, New York.

Gaarskjaer, F.B., 1978. Organization of the mossy fiber system of the rat studied in extended hippocampi: I. Terminal area related to number of granule and pyramidal cells. J. Comp. Neurol. 178, 49–72.

Golgi, C., Bentivoglio, M., Swanson, L., 2001. On the fine structure of the pes hippocampi major (with plates xiii–xxiii). 1886. Brain Res. Bull. 54, 461–483.

Harris, K.R., Woolf, L.A., 1980. Pressure and temperature-dependence of the self-diffusion coefficient of water and O-18 water. J. Chem. Soc., Faraday Trans., I 76, 377–385.

Larson, E.B., Kukull, W.A., Katzman, R.L., 1992. Cognitive impairment: dementia and Alzheimer's disease. Annu. Rev. Public Health 13, 431–449.

Lorente de No, R., 1934. Studies on the structure of the cerebral cortex: II. Continuation of the study of the ammonic system. J. Psychol. Neurol. 46, 113–177.

Ma, Y., Hof, P.R., Grant, S.C., Blackband, S.J., Bennett, R., Slatest, L., McGuigan, M.D., Benveniste, H., 2005. A three-dimensional digital atlas database of the adult c57bl/6j mouse brain by magnetic resonance microscopy. Neuroscience 135, 1203–1215.

McBain, C.J., Traynelis, S.F., Dingledine, R., 1990. Regional variation of extracellular space in the hippocampus. Science 249, 674–677.

Nadler, J.V., 2003. The recurrent mossy fiber pathway of the epileptic brain. Neurochem. Res. 28, 1649–1658.

Özarslan, E., Vemuri, B.C., Mareci, T.H., 2005. Generalized scalar measures for diffusion MRI using trace, variance, and entropy. Magn. Reson. Med. 53, 866–876.

Paxinos, G., Watson, C., 1986. The Rat Brain in Stereotaxic Coordinates, 2nd ed. Academic Press, New York.

Pellegrino, L.J., Cushman, A.J., 1967. A Stereotactic Atlas of the Rat Brain. Meredith Publishing Company, New York.

Pierpaoli, C., Basser, P.J., 1996. Toward a quantitative assessment of diffusion anisotropy. Magn. Reson. Med. 36, 893–906.

Press, W.H., Teukolsky, S.A., Vetterling, W.T., Flannery, B.P., 1992. Numerical Recipes in {C}: The Art of Scientific Computing. Cambridge Press, Cambridge.

Schmidt-Kastner, R., Freund, T.F., 1991. Selective vulnerability of the hippocampus in brain ischemia. Neuroscience 40, 599–636.

Shepherd, T.M., Thelwall, P.E., King, M.A., Wirth, E.D., Blackband, S.J., 2004. Cytoarchitectural basis for water diffusion in rat hippocampal slices. Proc. Int. Soc. Magn. Reson. Med. 12, 1231.

Shepherd, T.M., Thelwall, P.E., Stanisz, G.J., Blackband, S.J., 2005. Chemical fixation alters the water microenvironment in rat cortical brain slices—implications for MRI contrast mechanisms. Proc. Int. Soc. Magn. Reson. Med. 13, 619.

Spielmeyer, W., 1925. Zur pathogenese ortlich elektiver gehirnveranderungen. Z. Ges. Neurol. Psychiat. 99, 756–776.

Squire, L.R., Stark, C.E., Clark, R.E., 2004. The medial temporal lobe. Annu. Rev. Neurosci. 27, 279–306.

Sutula, T., Cascino, G., Cavazos, J., Parada, I., Ramirez, L., 1989. Mossy fiber synaptic reorganization in the epileptic human temporal lobe. Ann. Neurol. 26, 321–330.

Sykova, E., Mazel, T., Hasenohrl, R.U., Harvey, A.R., Simonova, Z., Mulders, W.H., Huston, J.P., 2002. Learning deficits in aged rats related to decrease in extracellular volume and loss of diffusion anisotropy in hippocampus. Hippocampus 12, 269–279.

Tauck, D.L., Nadler, J.V., 1985. Evidence of functional mossy fiber sprouting in hippocampal formation of kainic acid-treated rats. J. Neurosci. 5, 1016–1022.

Tuch, D.S., Reese, T.G., Wiegell, M.R., Makris, N., Belliveau, J.W., Wedeen, V.J., 2002. High angular resolution diffusion imaging reveals intravoxel white matter fiber heterogeneity. Magn. Reson. Med. 48, 577–582.

Van Hoesen, G.W., Hyman, B.T., 1990. Hippocampal formation: anatomy and the patterns of pathology in Alzheimer's disease. Prog. Brain Res. 83, 445–457.

Wakana, S., Jiang, H., Nagae-Poetscher, L.M., Van Zijl, P.C., Mori, S., 2004. Fiber tract-based atlas of human white matter anatomy. Radiology 230, 77–87.

Witter, M.P., Wouterlood, F.G., Naber, P.A., Van Haeften, T., 2000. Anatomical organization of the parahippocampal–hippocampal network. Ann. N. Y. Acad. Sci. 911, 1–24.

Woermann, F.G., Barker, G.J., Birnie, K.D., Meencke, H.J., Duncan, J.S., 1998. Regional changes in hippocampal T2 relaxation and volume: a quantitative magnetic resonance imaging study of hippocampal sclerosis. J. Neurol., Neurosurg. Psychiatry 65, 656–664.

Zhang, J., Van Zijl, P.C., Mori, S., 2002. Three-dimensional diffusion tensor magnetic resonance microimaging of adult mouse brain and hippocampus. NeuroImage 15, 892–901.